

Reduction of threshold current density for current-driven domain wall motion by shape control

A. Yamaguchi, K. Yano, H. Tanigawa, S. Kasai and T. Ono

Institute for Chemical Research, Kyoto University, Uji, 611-0011, Japan

KEYWORDS: current-driven domain wall motion, shape control, threshold current density

Abstract

We investigated the aspect ratio (thickness/width) dependence of the threshold current density required for the current-driven domain wall (DW) motion for the Ni₈₁Fe₁₉ nanowires. It has been shown theoretically that the threshold current density is proportional to the product of the hard-axis magnetic anisotropy K_{\parallel} and the DW width λ . (Phys. Rev. Lett. **92**, 086601 (2004).) We show experimentally that K_{\parallel} can be controlled by the magnetic shape anisotropy in the case of the Ni₈₁Fe₁₉ nanowires, and that the threshold current density increases with an increase of $K_{\perp} \cdot \lambda$. We succeeded to reduce the threshold current density by half by the shape control.

1. Introduction

The current-driven domain wall (DW) motion has attracted much attention from the viewpoint of application because this effect makes it possible to switch the magnetic configuration without an external magnetic field^{1), 2)}. It has been convincingly confirmed by series of experiments on magnetic thin films³⁻⁸⁾ and magnetic nanowires⁹⁻²⁰⁾. However, the threshold current densities required for the current-driven DW motion (J_C) are still high, $10^{11} - 10^{12} \text{ A/m}^2$ for the single ferromagnetic metal layer circuits⁹⁻¹⁶⁾ and the order of 10^{10} A/m^2 for the spin-valve ferromagnetic nanowires¹⁷⁻¹⁹⁾. Though the lower J_C of 10^9 A/m^2 has been reported for ferromagnetic semiconductor (Ga,Mn)As²⁰⁾, the Curie temperature of this material is below room temperature. Thus, it is indispensable to explore a way to reduce J_C for ferromagnetic metals from the viewpoint of practical applications.

It has been suggested theoretically that J_C is proportional to the product of the hard-axis magnetic anisotropy K_{\perp} and the DW width λ in the case of a thick DW and a weak pinning²¹⁾. Here, the thick DW means that the thickness of the DW is much larger than the Fermi wavelength of conduction electrons which is satisfied in usual ferromagnetic metals, and the weak pinning means that a pinning potential for a DW is much smaller than K_{\perp} / α , where α is the Gilbert damping factor. Thus, the theory predicts that J_C can be reduced by reducing K_{\perp} . For samples of Ni₈₁Fe₁₉, K_{\perp} can be controlled by the sample shape, because the crystal magnetic anisotropy of Ni₈₁Fe₁₉ is negligibly small and the magnetic anisotropy is dominated by the magnetostatic energy. In this letter, we show experimentally that J_C depends on the cross-sectional shape of Ni₈₁Fe₁₉ wires. Effect of the Joule heating of the sample is also discussed.

2. Experimental Details

Samples with two types of shape, L-shaped and semicircular-shaped magnetic wires of $\text{Ni}_{81}\text{Fe}_{19}$, were fabricated onto the thermally oxidized Si and MgO substrates by means of electron beam lithography and a liftoff method as shown in Figs. 1(a) and 1(b). We have checked that two types of wires on the same substrate have the same J_C when they have the same thickness and the same width. Samples investigated in this study are summarized in Table 1 with the experimental results. The widths of the wires were determined by means of a scanning electron microscope, and the thicknesses were determined by means of an atomic force microscope.

A single DW was introduced into a magnetic wire by the following procedure. For L-shaped wires, the direction of an external magnetic field was set about 30° from the wire axis in the substrate plane in order to introduce the DW at the position a little bit away from the corner (Fig. 1(a)). First, a magnetic field of +2 kOe was applied in order to align the magnetization in one direction along the wire. Then, a single DW was introduced by applying a magnetic field of -175 Oe¹³⁾. In the case of the semicircular-shaped wires, a magnetic field of 20 kOe was applied in the y-direction in the substrate plane and it was decreased to zero (Fig. 2(b)). Then, a single DW was introduced spontaneously around the center of the semicircular-shaped wire²²⁾.

The threshold current densities were determined by direct observations of the current-driven DW motion by using a magnetic force microscope (MFM) at room temperature^{13), 15)}. After the DW introduction, a pulsed current with duration of 5 μs was applied through the wire in the absence of a magnetic field. The current density of the pulsed current was increased until the DW was displaced in the opposite direction of the pulsed current. CoPtCr low moment probes were used in order to minimize the

influence of the stray field from the probe on the DW in the wire.

Magnetic anisotropies of the samples were determined by measuring the magnetoresistance effect. In narrow ferromagnetic wires, the magnetization is restricted to direct parallel to the wire axis due to the magnetic shape anisotropy. When a magnetic field is applied perpendicular to the wire axis, the magnetization is tilted from the wire axis and the angle between the magnetization and the measuring electric current increases. This causes the decrease in resistance and the resistance becomes minimum value when the magnetization directs parallel to the external magnetic field, because the $\text{Ni}_{81}\text{Fe}_{19}$ shows the anisotropic magnetoresistance (AMR) effect. Thus, the saturation magnetic field can be determined by the magnetoresistance measurement. We refer the saturation fields along the two magnetic hard axes to $H_{S//}$ and $H_{S\perp}$, respectively, as schematically shown in Fig. 1(c).

3. Results and Discussion

The results of the magnetoresistance measurements at 300 K for the samples #1, #2, #3, and #4 in Table 1 are shown in the inset of Fig. 2. The magnetic field was applied perpendicular to the substrate plane. As indicated by the arrows, H_S decreases monotonically with increasing the thickness of the wire. It should be noted that the sum of $\mu_0 H_{S//}$ and $\mu_0 H_{S\perp}$ for each sample was about 1.1 T, which is the saturation magnetization of $\text{Ni}_{81}\text{Fe}_{19}$ (M_S). This suggests that the shape anisotropy dominates the magnetic anisotropy in the samples. Because $H_{S//}$ in the semicircular-shaped wire can not be determined by measuring the magnetoresistance effect under a magnetic field in the plane because of its shape, we defined $\mu_0 H_{S//}$ as the difference between the saturation

magnetization and $\mu_0 H_{S\perp}$, $\mu_0 H_{S//} = M_S - \mu_0 H_{S\perp}$. This can be justified because the radius of the semicircular-shaped wire is much larger than both thickness and width of the wires. The hard-axis magnetic anisotropy $S^2 K_{\perp} / a^3$ in ref. 21 is expressed by experimentally obtained values as

$$\frac{S^2 K_{\perp}}{a^3} = M_s \cdot |H_{s\perp} - H_{s//}|, \quad (1)$$

where S and a is the localized spin and the lattice constant, respectively. Figure 2 shows $S^2 K_{\perp} / a^3$ as a function of the aspect ratio (thickness/width). $S^2 K_{\perp} / a^3$ decreased systematically with an increase of the aspect ratio. MFM observations under a magnetic field revealed that the samples had the depinning fields in the range from 15 to 100 Oe, suggesting that the pinning potentials in the wires were much smaller than K_{\perp} / α and the samples were in the weak pinning regime.

The high current density required for the current-driven domain wall motion inevitably causes the considerable Joule heating as previously reported²³⁾. We estimated the sample temperature during the application of the pulsed-current by using the method described in ref. 23. Figure 3 shows the estimated temperatures for the samples #6 and #9 as a function of the current density. The shape of these two wires was almost the same, but the estimated temperature of the wire on the thermally oxidized Si substrate (sample #6) was higher than that of the wire on the MgO substrate (sample #9) at the same current density. This is because MgO has the higher thermal conductivity than SiO_2 . J_C for each sample is indicated by the arrow in Fig. 3. J_C of the wire on the thermally oxidized substrate was much smaller than that of the wire on MgO substrate in spite of the similar dimension of the two wires. This can be attributable to the

reduction of M_S due to the higher sample temperature at J_C for the sample on the thermally oxidized substrate. The reduction of M_S results in the decrease of $S^2 K_{\perp} / a^3$ through eqn. (1), leading to the reduction of J_C . This indicates that we should take account of the decrease the saturation magnetization due to the Joule heating.

Figure 4 shows J_C as a function of $S^2 K_{\perp_{\text{eff}}} \cdot \lambda / a^3$, which was calculated by eqn. (1) by taking the reduction of M_S into account. DW width, λ , was calculated by the micromagnetic simulation OOMMF²⁴⁾. The parameters used for the calculation were cell size of 5 nm, a reduced saturation magnetization due to the heating, and a damping constant of $\alpha = 1$. As shown in Fig. 4, J_C increases with $S^2 K_{\perp_{\text{eff}}} \cdot \lambda / a^3$ and has a minimum value for $S^2 K_{\perp_{\text{eff}}} \cdot \lambda / a^3 = 0$, which is about half of the previously reported value for 10 nm-thick Ni₈₁Fe₁₉ wire with width of 240 nm^{13), 23)}. The tendency that J_C increases with $S^2 K_{\perp_{\text{eff}}} \cdot \lambda / a^3$ is qualitatively consistent with the theory²¹⁾, indicating that the spin-transfer is a most probable mechanism. However, the theory predicts much larger J_C than the experimental values. One possible reason of this discrepancy between the theory and the experiments is the internal spin structure of a DW; the theory assumes a simple one-dimensional DW, while a DW in the experiments has a complicated internal spin structure as previously reported^{10), 13)}. Another possibility is the existence of the field-like as suggested by recent theories²⁵⁻²⁸⁾.

4. Conclusion

We have shown that the threshold current density can be decreased by the reduction of the effective K . The smallest threshold current density was about half of the previously reported value for 10 nm-thick Ni₈₁Fe₁₉ wire with width of 240 nm^{13), 23)}, and this shows the effectiveness of the shape control. It was also suggested that the decrease in the saturation magnetization by sample heating plays a role for the reduction of the threshold current density.

Acknowledgements

The authors are grateful to G. Tatara, H. Kohno, and Y. Nakatani for valuable discussions. The present work was partly supported by MEXT Grants-in-Aid for Scientific Research in Priority Areas, JSPS Grants-in-Aid for Scientific Research, and Industrial Technology Research Grant Program in '05 from NEDO of Japan.

Reference

- (1) L. Berger, *J. Appl. Phys.* **55**, 1954 (1984).
- (2) L. Berger, *J. Appl. Phys.* **71**, 2721 (1992).
- (3) P. P. Freitas and L. Berger, *J. Appl. Phys.* **57**, 1266 (1985).
- (4) C. -Y. Hung and L. Berger, *J. Appl. Phys.* **63**, 4276 (1988).
- (5) C. -Y. Hung, L. Berger and C. Y. Shih, *J. Appl. Phys.* **67**, 5941 (1990).
- (6) E. Salhi and L. Berger, *J. Appl. Phys.* **73**, 6405 (1993).
- (7) L. Gan, S. H. Chung, K. H. Ashenbach, M. Dreyer, and R. D. Gomez, *IEEE Trans. Magn.* **36**, 3047 (2000).
- (8) H. Koo, C. Kraft, and R. D. Gomez, *Appl. Phys. Lett.* **81**, 862 (2002).
- (9) M. Kläui, C. A. F. Vaz, J. A. C. Bland, W. Wemsdorfer, G. Faini, E. Cambril, and L. J. Heyderman, *Appl. Phys. Lett.* **83**, 105 (2003).
- (10) M. Kläui, C. A. F. Vaz, J. A. C. Bland, W. Wemsdorfer, G. Faini, E. Cambril, L. J. Heyderman, F. Nolting, and U. Rüdiger, *Phys. Rev. Lett.* **94**, 106601 (2005).
- (11) T. Kimura, Y. Otani, K. Tsukagoshi, and Y. Aoyagi, *J. Appl. Phys.* **94**, 7947 (2003).
- (12) M. Tsoi, R. E. Fontana, and S. S. Parkin, *Appl. Phys. Lett.* **83**, 2617 (2003).
- (13) A. Yamaguchi, T. Ono, S. Nasu, K. Miyake, K. Mibu, and T. Shinjo, *Phys. Rev. Lett.* **92**, 077205 (2004).
- (14) N. Vernier, D. A. Allwood, D. Atkinson, M. D. Cooke, and R. P. Cowburn, *Europhys. Lett.* **65**, 526 (2004).
- (15) S. H. Florez, C. Kraft, and R. D. Gomez, *J. Appl. Phys.* **97**, 10C705 (2005).
- (16) M. Kläui, P. -O. Jubert, R. Allenspach, A. Bischof, J. A. C. Bland, G. Faini, U. Rüdiger, C. A. F. Vaz, L. Vila, and C. Vouille, *condmat/0504427*.

(17) J. Grollier, D. Lacour, V. Cros, A. Hamzić, A. Vaurès, A. Fert, D. Adam, and G. Faini, *J. Appl. Phys.* **92**, 4825 (2002).

(18) J. Grollier, P. Boulenc, V. Cros, A. Hamzić, A. Vaurès, A. Fert, and G. Faini, *Appl. Phys. Lett.* **83**, 509 (2003).

(19) C. K. Lim, T. Devolder, C. Chappert, J. Grollier, V. Cros, A. Vaurès, A. Fert, and G. Faini, *Appl. Phys. Lett.* **84**, 2820 (2004).

(20) M. Yamanouchi, D. Chiba, F. Matsukura, and H. Ohno, *Nature* **428**, 539 (2004).

(21) G. Tatara and H. Kohno, *Phys. Rev. Lett.* **92**, 086601 (2004).

(22) E. Saitoh, H. Miyajima, T. Yamaoka, and G. Tatara, *Nature* **432**, 203 (2004).

(23) A. Yamaguchi, S. Nasu, H. Tanigawa, T. Ono, K. Miyake, K. Mibu, and T. Shinjo, *Appl. Phys. Lett.* **86**, 012511 (2005).

(24) <http://math.nist.gov/oommf/>.

(25) A. Thiaville, Y. Nakatani, J. Miltat, and Y. Suzuki, *Europhys. Lett.* **69**(6), 990 (2005).

(26) S. Zhang and Z. Li, *Phys. Rev. Lett.* **93**, 127204 (2004).

(27) X. Waintal and M. Vert, *Europhys. Lett.* **65**, 427 (2004).

(28) S. E. Barnes and S. Maekawa, *Phys. Rev. Lett.* **95**, 107204 (2005).

Figure caption

Figure 1(a) Schematic illustration of a top view of the L-shaped wire. (b) Schematic illustration of a top view of the semicircular-shaped wire. (c) The magnetic easy axis is parallel to the wire axis. Two magnetic hard axes are perpendicular to the wire axis. One is in the substrate plane, and the other is perpendicular to the substrate plane.

Figure 2 The hard-axis magnetic anisotropy $S^2 K_{\perp} / a^3 = M_s \cdot |H_{s\perp} - H_{s//}|$ as a function of the aspect ratio (thickness/width). The solid squares, the solid circles, and the solid triangles indicate the results for the semicircular-shaped wires on MgO substrate, the L-shaped wires on the thermally oxidized Si substrates, and the semicircular-shaped wires on the thermally oxidized Si substrates, respectively. The inset is the results of the magnetoresistance measurements at 300 K for the samples #1, #2, #3, and #4. The magnetic field was applied perpendicular to the substrate plane. The magnetization saturation fields are pointed by the arrows.

Figure 3 The estimated temperatures for the samples #6 and #9 as a function of the current density.

Figure 4 The experimentally determined J_C as a function of the hard-axis magnetic anisotropy $S^2 K_{\perp_{\text{eff}}} \cdot \lambda / a^3$. The solid squares, the solid circles, and the solid triangles indicate the results for the semicircular-shaped wires on MgO substrate, the L-shaped wires on the thermally oxidized Si substrates, and the semicircular-shaped wires on the thermally oxidized Si substrates, respectively.

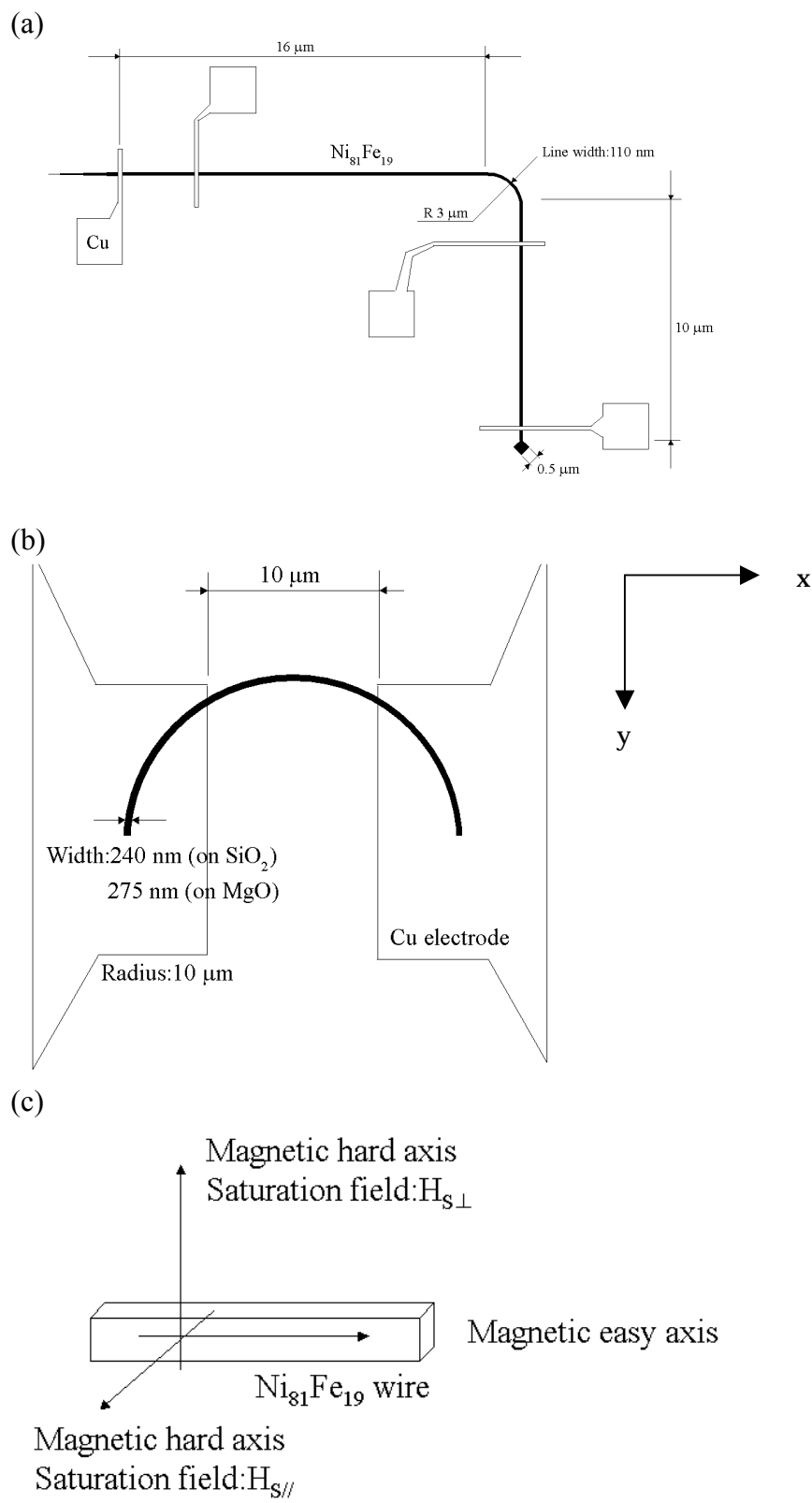


Fig. 1_Yamaguchi_et_al.

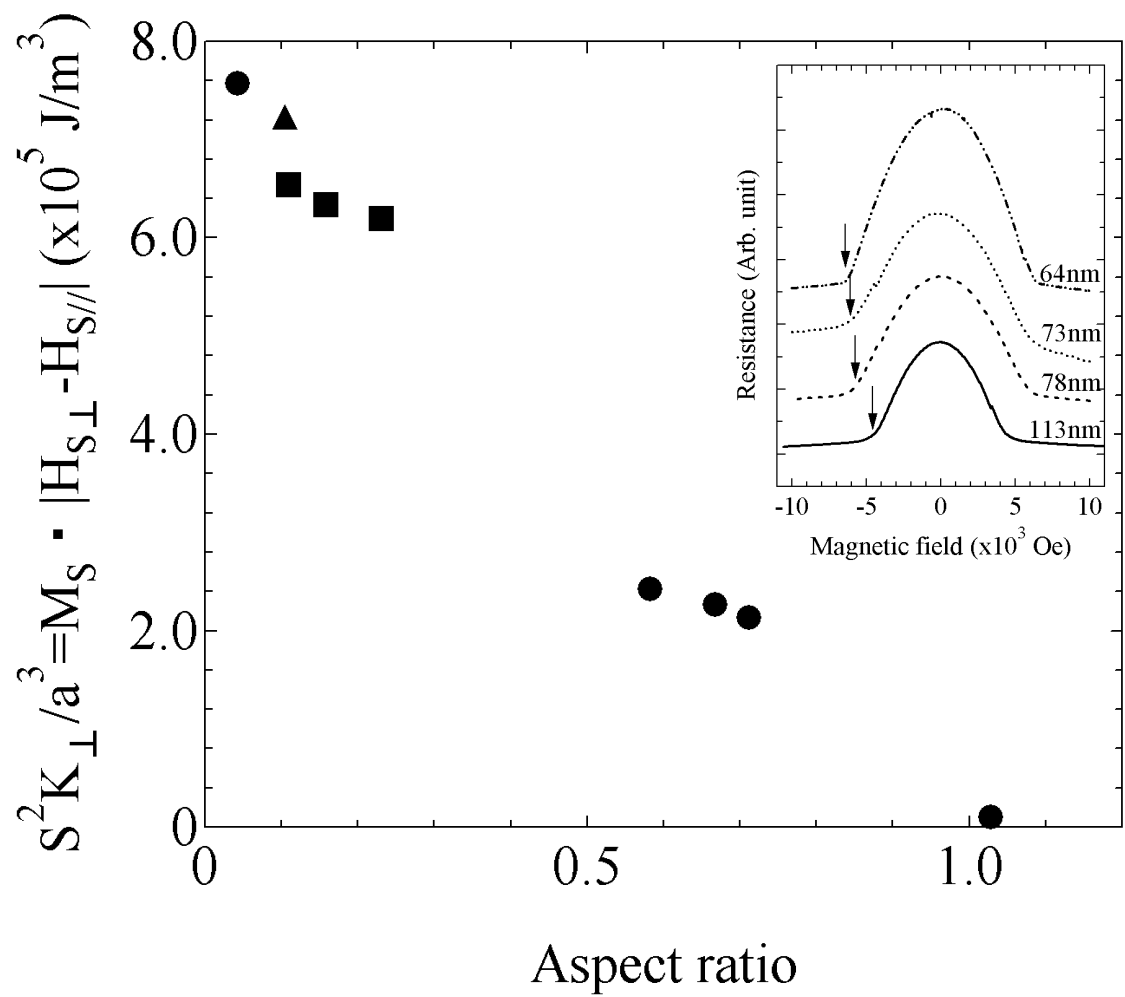


Fig. 2_Yamaguchi_et_al.

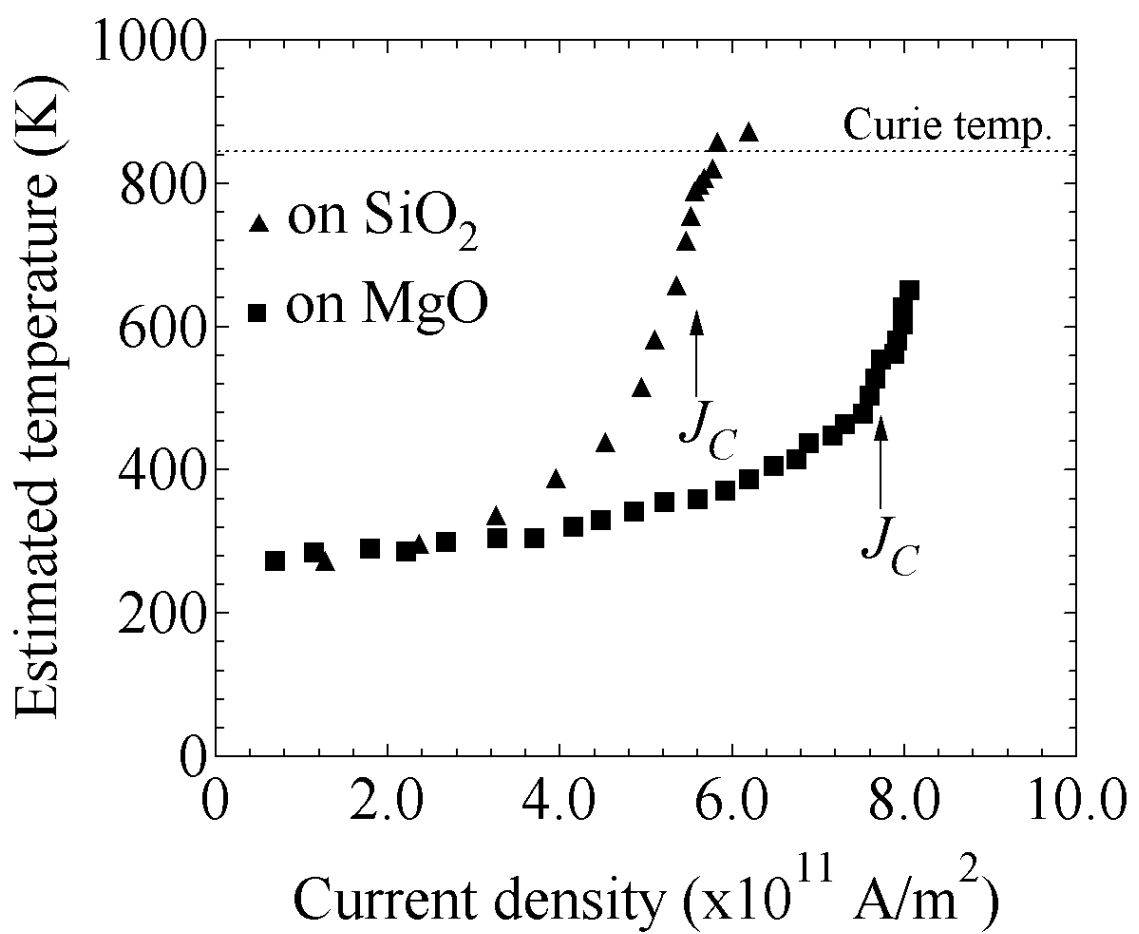


Fig. 3_Yamaguchi_et_al.

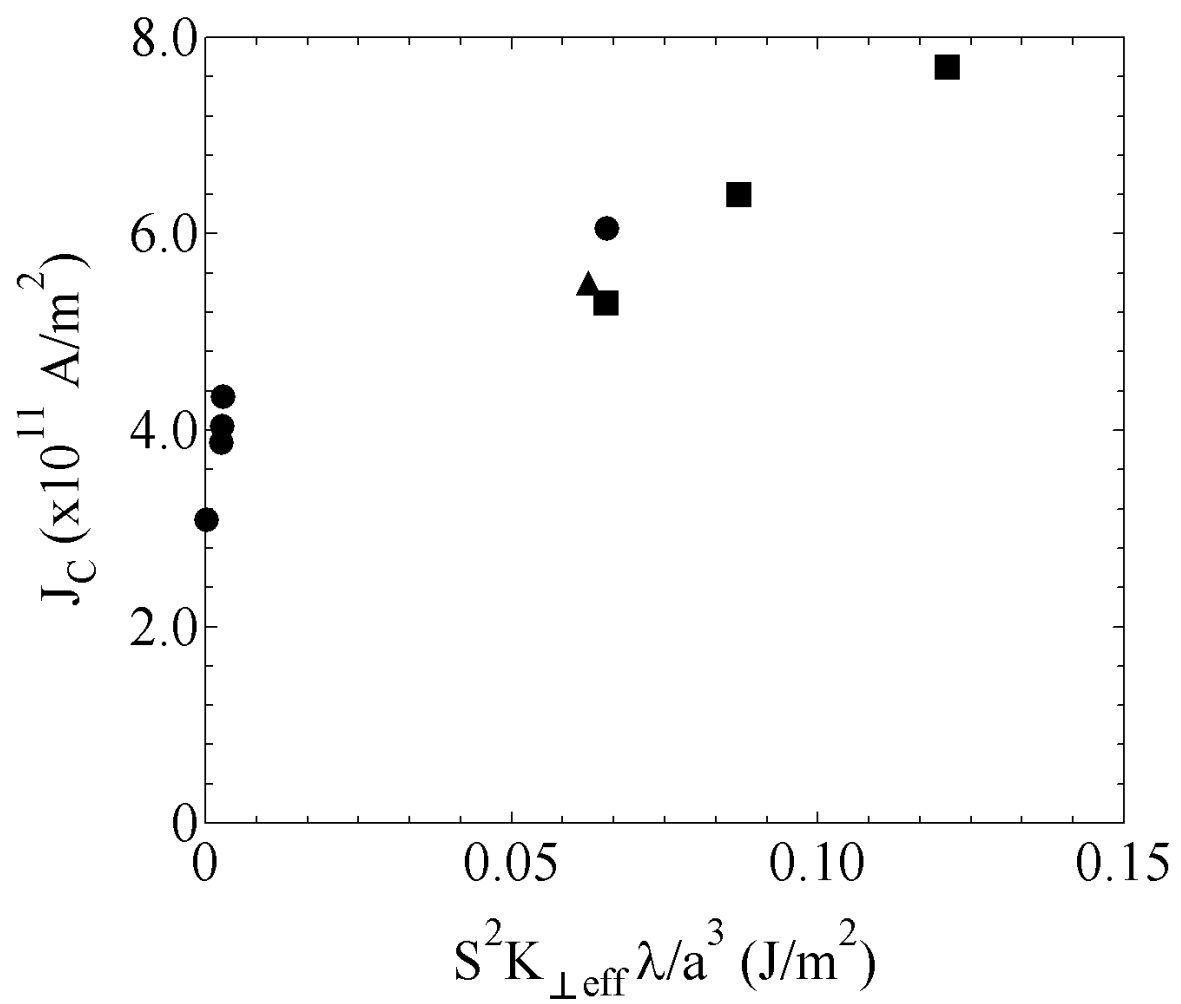


Fig. 4_Yamaguchi_et_al.

Table I. Summary of the samples and the experimental results.

Sample	Substrate	Type	Width (nm)	Thickness (nm)	Temperature (K)	M/M_s **	J_C ($\times 10^{11} \text{ A/m}^2$)
#1	SiO ₂	L	110	64	820	0.33	4.34
#2	SiO ₂	L	110	73	820	0.33	4.04
#3	SiO ₂	L	110	78	820	0.33	3.88
#4	SiO ₂	L	110	113	820	0.33	3.09
#5	SiO ₂	L	240	10	750	0.60	6.06
#6	SiO ₂	C	240	25	750	0.60	5.50
#7	MgO	C	130	30	400	0.90	5.30
#8	MgO	C	190	30	520	0.85	6.40
#9	MgO	C	275	30	550	0.82	7.70

*Type L and C correspond to the L-shaped and semicircular-shaped wire, respectively.

**Temperature and magnetization at the threshold current density.